

Synthesis and magnetic characterization of $\text{TmCo}_2\text{B}_2\text{C}$

M. ElMassalami, R. E. Rapp, F. A. B. Chaves and R. Moreno

Instituto de Física, Universidade Federal do Rio de Janeiro,

Caixa Postal 68528, 21945-972 Rio de Janeiro, Brazil

H. Takeya

National Institute for Materials Science,

1-2-1 Sengen, Tsukuba, Ibaraki 305-0047, Japan

B. Ouladdiaf

Institut Laue-Langevin, B.P.156 ,38042 Grenoble Cedex 9, France

J. W. Lynn, Q. Huang

NIST Center for Neutron Research,

National Institute of Standards and Technology, Gaithersburg, MD 20899-6102

R. S. Freitas and N. F. Oliveria Jr.

Instituto de Física., Universidade de São Paulo,

Rua do Matão 187 Travessa R, Cidade Universitária,

05315-970 Sao Paulo, SP , Brasil

(Dated: November 12, 2018)

Abstract

A new quaternary intermetallic borocarbide $\text{TmCo}_2\text{B}_2\text{C}$ has been synthesized via a rapid-quench of an arc-melted ingot. Elemental and powder-diffraction analyses established its correct stoichiometry and single-phase character. The crystal structure is isomorphous to that of $\text{TmNi}_2\text{B}_2\text{C}$ ($I4/mmm$) and is stable over the studied temperature range. Above 7 K, the paramagnetic state follows the modified Curie-Weiss behavior ($\chi = C/(T-\theta) + \chi_0$) wherein $\chi_0 = 0.008(1)$ emu/mole and the temperature-dependent term reflecting the paramagnetism of the Tm subsystem: $\mu_{\text{eff}} = 7.6(2) \mu_{\text{B}}$ [in agreement with the expected value for a free Tm^{3+} ion] and $\theta = -4.5(3)$ K. Long range ferromagnetic order of the Tm sublattice is observed to develop around ~ 1 K. No superconductivity is detected in $\text{TmCo}_2\text{B}_2\text{C}$ down to 20 mK, a feature which is consistent with the general trend in the $\text{RCo}_2\text{B}_2\text{C}$ series. Finally, the influence of the rapid-quench process on the magnetism (and superconductivity) of $\text{TmNi}_2\text{B}_2\text{C}$ will be discussed and compared to that of $\text{TmCo}_2\text{B}_2\text{C}$.

PACS numbers: 74.70.Dd, 75.50.-y, 81.40.Rs

I. INTRODUCTION

The magnetic ordering temperature of a Tm^{3+} sublattice in a thulium-based intermetallic compound is, in general, lower than that of its isomorphous heavy rare-earth-based counterparts of the same series.¹ One usually attributes such a lowering to a smaller de Gennes factor, $(g-1)^2J(J+1)$, assuming that parameters such as electronic structure are not modified across the isomorphous series. On the other hand, for Tm-based compounds that belong to a family of different series, electronic properties (such as the position of the Fermi level within the density of states curve, the derivative of the density of states, spin fluctuations, ... etc.) do change and such a change can modify significantly the type, character, and critical point of the magnetic order. Such features are well documented in, say, the RM_2 family (R = magnetic rare earth, M = $3d$ transition metal):^{2,3,4,5} for the $\text{Tm}M_2$ compounds, the critical temperature of each member depends critically on the type of M but, nevertheless for each RM_2 series, it is always lower than that of the corresponding heavy R -isomorphs.

Another illustration which is of relevance to this work is the case of the heavier members of the borocarbide family RM_2B_2C . For the $R\text{Ni}_2B_2C$ series, the Neel temperatures (T_N) scale reasonably well with the de Gennes factor;^{6,7,8} moreover, both T_N (1.5 K) and the de Gennes factor (1.17) of TmNi_2B_2C are the lowest. In contrast, the critical points T_C of the isomorphous series $R\text{Co}_2B_2C$ do not show this scaling. Furthermore, T_C of TmCo_2B_2C has not, so far, been reported, though based on an extrapolation of T_C within the phase diagram of $R\text{Co}_2B_2C$ (T_C versus the de-Gennes factor), it is expected to be 2 K.⁹ But this would contradict the observed trend that T_C 's of the heavier members of $R\text{Co}_2B_2C$ are not higher than those of the corresponding $R\text{Ni}_2B_2C$. This question has not been addressed before due to the difficulties in the synthesis and stabilization of a single-phase TmCo_2B_2C compound. This work reports on the successful preparation as well as the structural and physical characterization of single-phase TmCo_2B_2C samples. The obtained results confirm that indeed its T_C is not higher than that of TmNi_2B_2C .

Two findings are of special interest to the understanding of the superconductivity, magnetism, and their interplay in the borocarbide family: First, no sign of superconductivity is observed down to 20 mK; such a result, together with the nonsuperconductivity of YCo_2B_2C ,^{9,10} indicate that the quench of the superconductivity in $R\text{Co}_2B_2C$ is related to the unfavorable spin fluctuation process (for the particular case of TmCo_2B_2C , there is, in

addition, the pair-breaking ferromagnetic, FM, order). Secondly, the long-range order of the localized $4f$ moments of $\text{TmCo}_2\text{B}_2\text{C}$ does not appear to be a spin density wave as in the case of $\text{TmNi}_2\text{B}_2\text{C}$; rather, we argue that a FM state is consistent with the results of the magnetization, specific heat, and neutron diffraction. These findings will be demonstrated and discussed in § III. Before that we describe, in § II, the synthesis process and show how the stoichiometry and the single-phase character of the rapid-quenched (rq) $\text{TmCo}_2\text{B}_2\text{C}$ and $\text{TmNi}_2\text{B}_2\text{C}$ samples were verified. An evaluation of the influence of the rate of the rq process on the studied physical properties of $\text{TmCo}_2\text{B}_2\text{C}$ (§ II) together with a detailed comparison of the properties of a normal-prepared, non-quenched (nq) $\text{TmNi}_2\text{B}_2\text{C}$ with those of a rq $\text{TmNi}_2\text{B}_2\text{C}$ (§ II) would allow us to extract the dominant influences of this rq process.

II. EXPERIMENT

A. rq - $\text{TmCo}_2\text{B}_2\text{C}$

A starting sample with a stoichiometry of $\text{TmCo}_2\text{B}_2\text{C}$ was prepared by a conventional arc-melt procedure under a highly pure (99.999%) argon atmosphere. The obtained product, when tested with X-ray diffraction, showed a multi-phase pattern. This same product, shaped into balls with diameters around 3–5 mm, was remelted and directly rapid-quenched by hitting it with a copper hammer.¹¹ The final product is a single-phase $\text{TmCo}_2\text{B}_2\text{C}$ in the form of thin flakes (50 ~ 100 μm thickness). Once obtained, the sample is stable in air and does not need special care during the handling or storing process, at least within an interval of months.

In contrast to the $R\text{Ni}_2\text{B}_2\text{C}$ series^{12,13} or even to other $R\text{Co}_2\text{B}_2\text{C}$ members,⁹ the rq process is essential for the synthesis of $\text{TmCo}_2\text{B}_2\text{C}$. Fig. 1 shows the diffractograms of two samples of $\text{TmCo}_2\text{B}_2\text{C}$ prepared with different quenching rates (the one with a faster quench rate is enriched with ^{11}B). These diffractograms together with results from various measuring techniques reveal that the rq process drastically diminishes the amount of impurity phases and as such leads to noticeable changes in the physical properties (see below, in particular Fig. 4). All measurements reported below were carried out on the same as-prepared, rapid-quenched, ^{11}B -enriched batch: conventional annealing (often followed for the borocarbides samples) leads to a surge of additional contaminations.

TABLE I: The molar ratios of the ^{11}B -enriched, rapid-quenched $\text{TmCo}_2\text{B}_2\text{C}$ and $\text{TmNi}_2\text{B}_2\text{C}$ samples. The calculations are based on the weight percentage data (normalized to the Tm content) and using the following atomic weights: $\text{Tm}=168.93421(3)$, $\text{Co}=58.93320(1)$, $\text{Ni}=58.6934$, $^{11}\text{B}=10.995$ (99.5% enriched from Eagle Pitcher Ind. Inc.), $\text{B}=10.811(5)$, and $\text{C}=12.011(1)$. The room-temperature cell parameters of $\text{TmCo}_2\text{B}_2\text{C}$, as obtained from XRD analysis (see Fig. 1), are $a=3.473(1)\text{\AA}$, $c=10.647(4)\text{\AA}$. For $\text{TmNi}_2\text{B}_2\text{C}$, see Table II.

| compound | ratio | Tm | Co | Ni | B | C |
|-----------------------------------|-------|---------|----------|----------|---------|---------|
| $\text{TmCo}_2\text{B}_2\text{C}$ | % | 52.2(1) | 36.3(1) | - | 6.69(1) | 3.81(1) |
| | molar | 1 | 1.993(5) | - | 1.97(3) | 1.03(3) |
| $\text{TmNi}_2\text{B}_2\text{C}$ | % | 52.8(1) | - | 36.0(1) | 6.39(1) | 3.77(1) |
| | molar | 1 | - | 1.962(6) | 1.86(3) | 1.00(3) |

The elemental analysis of both $rq\text{-TmCo}_2\text{B}_2\text{C}$ and $rq\text{-TmNi}_2\text{B}_2\text{C}$ is shown in Table I. The content of Tm, Co, and B were determined by the Induction Coupled Plasma analysis while that of C by the process of carbon combustion followed by Infrared absorption analysis. Table I shows also the cell parameters as obtained from room-temperature X-ray diffraction analysis [Fig. 1 (b)]. As can be verified, these results (in particular that of B and C) do confirm the correct stoichiometry of the $\text{TmCo}_2\text{B}_2\text{C}$ samples.

The crystal structure was studied by X-ray diffraction (room-temperature) and neutron diffraction ($0.36 < T < 30$ K). Physical characterizations were carried out with the following techniques: magnetization [$M(T, H)$, $0.5 < T < 30$ K, $H < 150$ kOe], dc susceptibility [$\chi_{dc}(T) = M/H$, $0.5 < T < 300$ K, $H \leq 10$ kOe], ac susceptibility [$\chi_{ac}(T)$, $0.02 < T < 20$ K, $f=200 \sim 1000$ Hz, $h_{ac} < 10$ Oe], and specific heat [$C(T)$, semi-adiabatic, $0.1 < T < 15$ K]. Neutron-diffraction was carried out at two different sites: (i) the Institut Laue-Langevin (ILL, Grenoble, France) using the D2B diffractometer ($3 \leq T \leq 30$ K) with a wavelength of $\lambda = 1.595 \text{\AA}$, and (ii) the National Institute of Standards and Technology (NIST, Gaithersburg, USA) using the high-resolution powder diffractometer ($\lambda = 2.0787 \text{\AA}$, $T=0.36$ K) and the BT-9 triple-axis instrument with a pyrolytic graphite monochromator and filter ($\lambda = 2.359 \text{\AA}$, $0.48 \leq T \leq 4.5$ K). Data were also collected on the new BT-7 triple axis spectrometer using the position sensitive detector in diffraction mode. For these neutron measurements a sample weighing 0.66 grams was used.

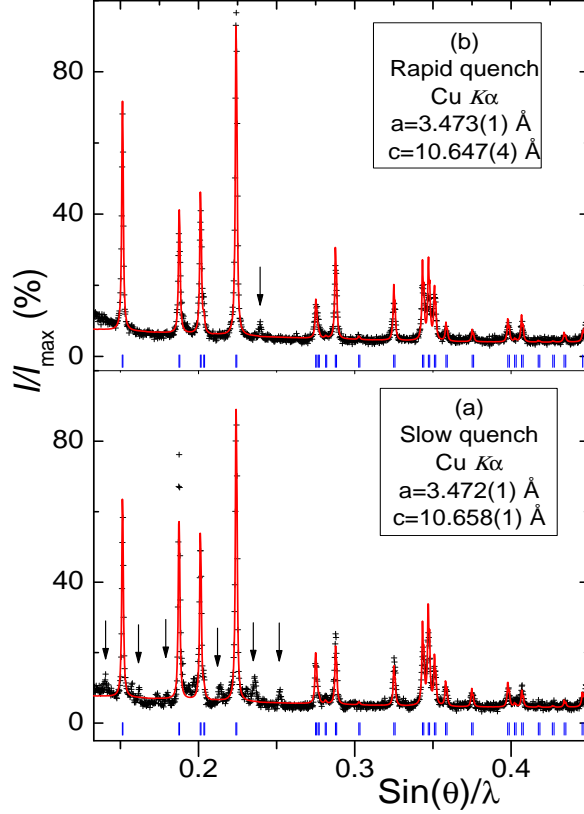


FIG. 1: (Color online) Room temperature X-ray diffractograms ($\text{Cu } K\alpha$) of (a) slow-quenched and (b) rapid-quenched $\text{TmCo}_2\text{B}_2\text{C}$. Rietveld analysis (solid lines) shows that the lattice parameters are hardly affected by the variation of the quench rate. Nevertheless, the impurity content are noticeably suppressed. On comparison with the neutron diffractograms (see later), allowance should be made for the difference in the f -factors.

B. rq - $\text{TmNi}_2\text{B}_2\text{C}$

Intended as a helpful guide in the evaluation of how much the properties of $\text{TmCo}_2\text{B}_2\text{C}$ are being influenced by the rq process, we investigated also the physical properties of a rq $\text{TmNi}_2\text{B}_2\text{C}$ sample and compare its results with those of the reported nq $\text{TmNi}_2\text{B}_2\text{C}$ sample. It is recalled that a nq $\text{TmNi}_2\text{B}_2\text{C}$ sample shows typical second-order-type superconducting and magnetic phase transitions occurring, respectively, at $T_c = 11$ K and $T_N = 1.5$ K.^{14,15} We synthesized a rq $\text{TmNi}_2\text{B}_2\text{C}$ via an identical preparation procedure as the one used for $\text{TmCo}_2\text{B}_2\text{C}$; the resulting sample has been studied by room-temperature XRD, specific heat, and magnetization measurements. The cell parameters and the paramagnetic CW behavior

TABLE II: Comparison between the room-temperature cell parameters (a , c), the z parameter indicating the position of the B atom (the positions of the other atoms are fixed by symmetry), and the paramagnetic Curie-Weiss parameters (figures not shown) of the rapid-quenched and non-quenched sample of $\text{TmNi}_2\text{B}_2\text{C}$. For the non-quenched sample, the cell parameters are taken from Lynn *et al.*⁸ while the CW parameters are from Cho *et al.*¹⁴

| $\text{TmNi}_2\text{B}_2\text{C}$ | a (Å) | c (Å) | z | $p_{eff}(\mu_B)$ | $\theta(\text{K})$ |
|-----------------------------------|-----------|-------------|-----------|------------------|--------------------|
| rapid-quenched | 3.4857(9) | 10.5609(27) | 0.3519 | 7.6(1) | -7.5(2) |
| non-quenched | 3.4866(2) | 10.5860(5) | 0.3598(2) | 7.54(2) | -11.6(4) |

(see Table II) reflect slight modifications which may be related to the rq process and a slight depletion in B content. It is noted that the rq process does not induce any noticeable moment on the Ni-sublattice.

Figure 2 shows that both the magnetic and superconducting order of $\text{TmNi}_2\text{B}_2\text{C}$ do survive the rq process (only that T_N and T_c are lowered to 1.2 K and 10 K, respectively) suggesting that the intrinsic forces that govern these cooperative phenomena are much stronger than the quench-induced disordering effects. Nevertheless, the rq process has modified substantially the structure of the curves within the transition region: the width of the superconducting phase transition [Fig. 2(a)] is substantially increased while the height (width) of the magnetic phase transition is strongly reduced (increased) to the extent that the magnetic transition is manifested as a weak, broadened event; the λ -type magnetic transition of the nq sample is being transformed by the rq process into an almost featureless event; in this case the phase change, in contrast to the nq case, is evidenced in the features of the first-order derivative: thus the rq process may modify the character and type of the magnetic phase transition. As we observed no hysteresis effects, the assignment of a first-order character to this phase transition is not unambiguous. At any rate, it can be safely concluded that the superconducting (and to some extent the magnetic) features of both the rq - and nq - $\text{TmNi}_2\text{B}_2\text{C}$, except for the region neighboring the critical temperature, are practically similar. It is then concluded that the tetragonal $\text{TmNi}_2\text{B}_2\text{C}$ structure, in sharp contrast with $\text{TmCo}_2\text{B}_2\text{C}$, is a low-temperature phase. Nevertheless, the observation that both isomorphs have almost the same structural-chemical properties suggests that the overall effect of the rq process on the physical properties of $\text{TmCo}_2\text{B}_2\text{C}$ would not differ much from the

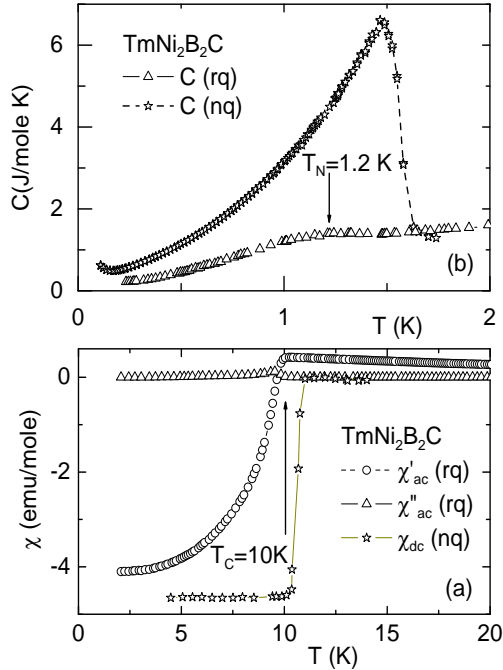


FIG. 2: (a) Low-temperature, low-field ac (χ_{ac}) and dc (χ_{dc}) susceptibilities of $\text{TmNi}_2\text{B}_2\text{C}$. χ_{ac} ($H_{ac} = 1$ Oe, $f = 500$ Hz) is measured on rq sample while χ_{dc} ($H_{dc} = 10$ Oe) is measured by Cho *et al.*¹⁴ on nq sample. (b) The total specific heats of rq and nq $\text{TmNi}_2\text{B}_2\text{C}$ samples. The later is taken from Movshovich *et al.*¹⁵ Note the large broadening of the superconducting and magnetic transitions of the rq samples.

trend observed in $\text{TmNi}_2\text{B}_2\text{C}$; in particular as that the rq process did not modify drastically the the intrinsic physical properties of $\text{TmNi}_2\text{B}_2\text{C}$, then both features of $\text{TmCo}_2\text{B}_2\text{C}$ (the nonsuperconductivity and the FM mode, see below) are considered to be intrinsic properties that are not strongly influenced by the rq process.

III. RESULTS AND DISCUSSION

The analysis of the powder diffractograms (Fig. 3 and Table III) indicates that $\text{TmCo}_2\text{B}_2\text{C}$ crystallizes in the tetragonal $\text{LuNi}_2\text{B}_2\text{C}$ -type structure which, within the experimental accuracy, is stable over the range $0.36 \leq T \leq 300\text{K}$. In comparison with isomorphous $\text{TmNi}_2\text{B}_2\text{C}$, the introduction of Co reduces the a -parameter and elongates the c -axis length but it induces no drastic shift in the B z -parameter (no particular significance is attributed to the observation that the z -parameters of both rq samples are 2% different from the nq

TmNi₂B₂C). It is reassuring that the obtained cell parameters, when plotted together with those of the other RCO_2B_2C compounds, evolve linearly with the effective metallic radius of the R atom (see Fig. 2 of Ref. 9).

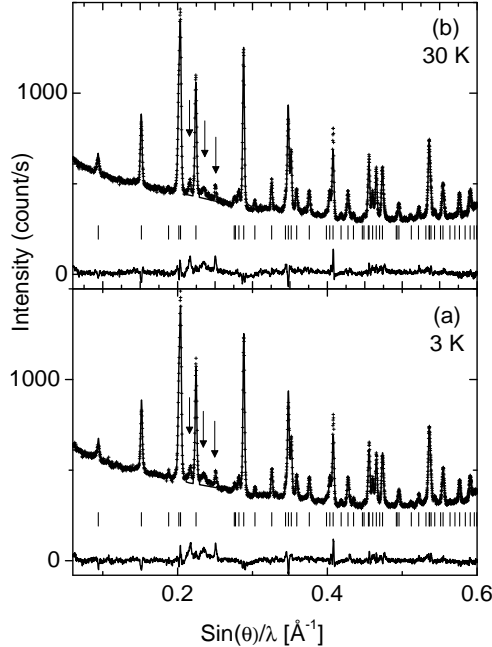


FIG. 3: Neutron powder diffractograms of TmCo₂B₂C, measured on D2B (ILL) diffractometer at (a) 3 K, and (b) 30 K. Note the very weak impurity lines at $\sin(\theta)/\lambda=0.217, 0.234, \text{ and } 0.251 \text{ \AA}^{-1}$ (see Fig. 1) The intensity of the strongest impurity line relative to that of the main phase amounts only to 4%.

A. Magnetic susceptibilities (ac and dc)

Thermal evolution of the isofield dc susceptibilities of the rq TmCo₂B₂C, $\chi_{dc} = M/H$ (Fig. 4), follows faithfully, down to 7 K, the modified Curie-Weiss (CW) behavior $\chi_{dc}(T) = C/(T - \theta) + \chi_0$, wherein $\mu_{eff} = 7.6(2) \mu_B$, $\theta = -4.5(3) \text{ K}$, and the temperature-independent paramagnetic (TIP) contribution $\chi_0 = 0.008(1) \text{ emu/mole}$. Similar high-temperature, modified CW paramagnetism is also manifested in the zero-field $\chi_{ac}(T > 7 \text{ K}) = \partial M / \partial H$ curve (Fig. 5). $\chi_{dc}(T)$ of a slow-quenched (sq) TmCo₂B₂C (shown also in Fig. 4) is higher in value and is not well described by the modified CW law. Based on the structural analysis, the difference among these two curves is related to the content of the contamination which,

TABLE III: Cell parameters (a, c) and the B-atom z -parameter of $\text{TmCo}_2\text{B}_2\text{C}$ at selected temperatures. The experimental diffractograms and the theoretically calculated patterns are shown in Figs. 3 and 9. In the Rietveld analysis of the diffractograms, the thermal parameters were found to be the same as those of $\text{TmNi}_2\text{B}_2\text{C}$ given in Lynn *et al.*⁸ while the occupation parameters gave similar values as the ones obtained from elemental analysis (see Table I)

| T (K) | a (Å) | c (Å) | z |
|---------|-----------|------------|-----------|
| 30 | 3.4684(2) | 10.6411(6) | 0.3597(2) |
| 3 | 3.4681(2) | 10.6413(7) | 0.3596(2) |
| 0.36 | 3.4689(2) | 10.6438(9) | 0.3587(3) |

in turn, is governed by the speed of the quenching rate (see Fig. 1): a faster rate leads to a reduction in contamination and, consequently, to a lowering in the magnetic susceptibility, in particular χ_0 . It is expected that on the limit of a faster quench, there would be no impurity's contribution and χ_0 would be much smaller but nonvanishing since χ_0 of $\text{YCo}_2\text{B}_2\text{C}$ is nonzero.¹⁶ Such a limit χ_0 may be due to a van Vleck-type contribution or an exchange-enhanced Pauli susceptibility. The admixture of high-lying orbitals into the ground state of the Tm^{3+} ion can be ruled out since no such effect is observed in $\text{TmNi}_2\text{B}_2\text{C}$ [Ref. 14] (not even in the rq -samples, see Table II). But such TIP is common in the cubic Laves $R\text{Co}_2$ phases^{2,3} wherein $\chi_0 \approx 0.004$ emu/mole. Though the above arguments as well as the similar argument on $\text{YCo}_2\text{B}_2\text{C}$ [Ref. 16] suggest that such an additional χ_0 may be related to the modification in the electronic structure of the $3d$ subband (as a result of the introduction of the Co atoms), however a final statement on this χ_0 should wait for a further analysis.

As the temperature is lowered towards and below the liquid helium point, both $\chi_{dc}(T)$ (Fig. 4) and $\chi_{ac}(T)$ (Fig. 5) manifest a rapid increase, going through a peak, and afterwards dropping weakly downwards. Considering that $\chi_{ac}(T)$ has an accentuated peak with a maximum at 0.8(1) K and that at this point $\chi_{dc}(T, 10 \text{ kOe})$ starts to decrease, such a point is taken to indicate a magnetic phase transition (see below).

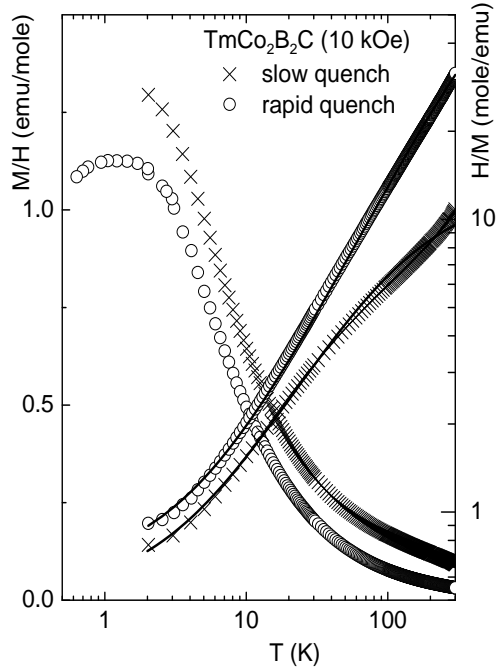


FIG. 4: Temperature-dependent $\chi_{dc} = M/H$ curves at $H=10$ kOe of $\text{TmCo}_2\text{B}_2\text{C}$. The temperature axis is logarithmic so as to emphasize the low-temperature part. The influence of the rate of the quenching process is demonstrated by comparison with a slow-quenched sample (see Fig. 1). The reciprocal χ_{dc} (right ordinate, logarithmic) for the *rq* sample (represented by circles) is well described by the modified CW behavior which is shown as solid lines (see text).

B. Magnetization

Magnetization isotherms (Fig. 6) show that even for a field of 150 kOe, the magnetic moment per unit formula reaches only $4.5 \pm 0.2 \mu_B$ ($T=0.65$ K) which is 65% of the value expected for a free Tm^{3+} ion. Such a high-field susceptibility is attributed to the magnetic response of the Co subsystem. The total moment saturation is estimated from the extrapolation $\lim_{1/H \rightarrow 0} M(H)$: the saturated moment (upper-left inset of Fig. 6) increases smoothly as the temperature is decreased. On the other hand, the M versus H/T curves (lower-right inset of Fig. 6) reveal that the isotherms at 1.4 and 2.5 K almost collapse on each other but that of 0.65 K is distinctly different. This observation supports our earlier arguments that $\text{TmCo}_2\text{B}_2\text{C}$ orders magnetically with an onset point lower than 1.4 K: within the paramagnetic state, all $M(H/T)$ curves follow the same Brillouin function and as such collapse on each other while below T_C , the rapid development of the ordered moment ensures that each

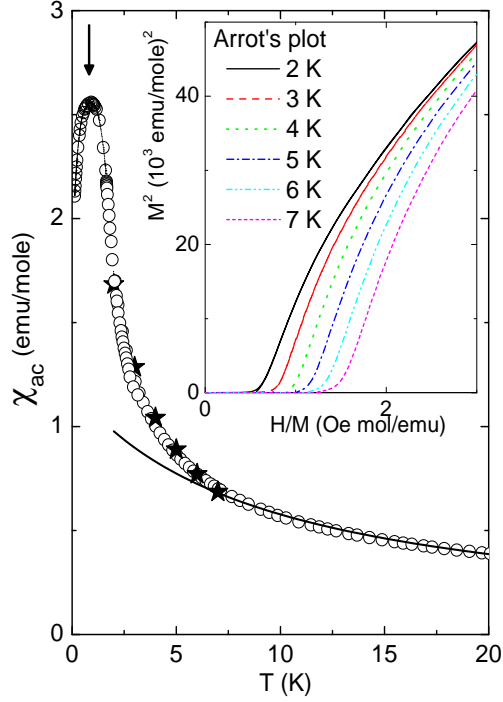


FIG. 5: (Color online) Thermal evolution of the zero-field $\chi_{ac}(T) = \partial M/\partial H$ of the *rq* $\text{TmCo}_2\text{B}_2\text{C}$. The solid line represents a fit to the same modified CW relation as in Fig. 3. The stars represent $(M/H)_{H \rightarrow 0}$ extrapolated from the Arrott's plots which are shown in the inset: the agreement indicates that the influence of the magnetic impurities within this range of temperatures is negligible.

of the $M(H/T)$ isotherms is distinctly different from one another and, in particular, from all paramagnetic isotherms.

Chang *et al.*¹⁷ observed that the moment of $\text{TmNi}_2\text{B}_2\text{C}$ increases as the temperature decreases; namely $\mu(1.2 \text{ K}) = 3.74 \mu_B$ and $\mu(50 \text{ mK}) = 4.8 \mu_B$. Comparing these features with those of Fig. 6, it is inferred that the magnitude and thermal evolution of the moments of both isotherms are similar which suggests a similarity in the low-lying CEF level scheme. As such it is expected that the orientation of the Tm moment to be along the *c* axis just as observed in $\text{TmNi}_2\text{B}_2\text{C}$. The observed difference in the Tm^{3+} moment strength of the two isomorphs may be due to a slight variation in the CEF effects. Rapid-quench influence on the site-occupation may lead to a reduction or even a complete collapse of the Tm moment (just as argued by Mulder *et al.*^{18,19} to explain the reduction of the Tm moment in $\text{TmNi}_2\text{B}_2\text{C}$).

The low-field part of the $M(H, 0.65 \text{ K})$ curve of Fig. 6 does not manifest those characteristic features (such as convex curvature at a spin flop event) which can be taken as

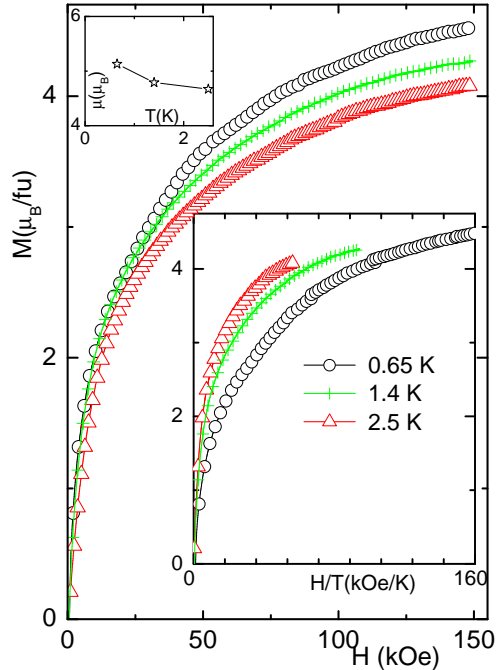


FIG. 6: (Color online) Magnetization isotherms $M(H)$ of $\text{TmCo}_2\text{B}_2\text{C}$ at different temperatures. The lower-right inset shows M versus H/T curves while the upper-left inset shows the saturated moment obtained from $\lim_{1/H \rightarrow 0} M(H)$. The lines are a guide to the eye (see text).

indicative of an AFM ground state; instead it shows a monotonic and steep increase which is typical of a forced magnetization of a FM-like state. It is not uncommon in the magnetism of the intermetallics that the character of the magnetic ground state is different from the one suggested by the sign of the Curie-Weiss temperature.

C. Specific Heat

The zero-field $C(T)$ curve of $\text{TmCo}_2\text{B}_2\text{C}$ is shown in Fig. 7. The low-temperature part of the total $C(T)$ is largely due to the magnetic contribution, $C_M(T)$, which is obtained after subtracting the contributions due to both the diamagnetic reference ($\text{YCo}_2\text{B}_2\text{C}$, Ref.9) and the nuclear interaction ($C_N \approx 3.5T^{-2}$ mJ/mole K). It is interesting to note that the associated hyperfine interaction (and the electronic magnetic moment) is much smaller than that of Tm-metal ($C_N \approx 26.8T^{-2}$ mJ/mole K),²⁰ but closer, as expected, to that of $\text{TmNi}_2\text{B}_2\text{C}$ ($C_N \approx 4.8T^{-2}$ mJ/mole K).¹⁵

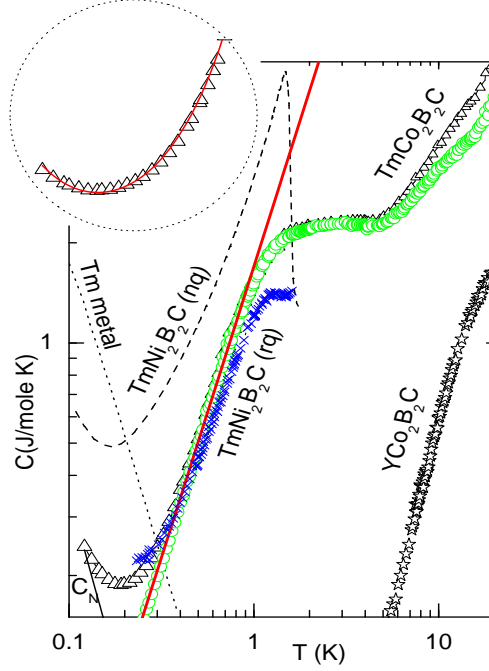


FIG. 7: (Color online) The specific heat curve (triangles) of $\text{TmCo}_2\text{B}_2\text{C}$. For comparison, we include the specific heat of $\text{YCo}_2\text{B}_2\text{C}$ [stars, Ref. 16], the non-quenched $\text{TmNi}_2\text{B}_2\text{C}$ (dashed line, Ref. 15), the rapid-quench $\text{TmNi}_2\text{B}_2\text{C}$ (cross, Fig.1), and (only the nuclear contribution of) the Tm-metal (dotted line, Ref. 20). The magnetic contribution (circles) and the empirical function $C_M(T)=1.7T^{\frac{7}{4}}$ J/moleK (thick solid line) are also indicated (see text). The inset shows an expansion of the low-temperature tail of the total specific heat of $\text{TmCo}_2\text{B}_2\text{C}$ (triangles) together with $C_{tot} = C_{ep}(\text{YCo}_2\text{B}_2\text{C}) + 0.035T^{-2} + 1.7T^{\frac{7}{4}}$ J/molK (solid line).

Figures 7-8 show that $C_M(T < 0.8 \text{ K}) = 1.7T^{\frac{7}{4}}$ J/mole K; above 0.8 K it turns slowly into a plateau which extends up to 5 K; above this temperature it resumes the monotonic increase but with a slower rate. This power-type thermal evolution of $C_M(T)$ (with an exponent being close to $\frac{3}{2}$) is consistent with what one would expect from a magnon contribution of a FM ordered state wherein the dispersion relation is quadratic and the anisotropic field is vanishingly small.^{21,22}

The magnetic entropy (Fig. 8) evolves as $S_M(T < 0.8 \text{ K}) = 0.85T^{\frac{7}{4}}$ J/mole K, increases steadily for $T > 0.8 \text{ K}$, and approximates the doublet-value $R \ln(2)$ only above 8 K. As all contributions from the Co subsystem has already been subtracted, then this entropy contribution must be due solely to the Tm subsystem and as such the lowest-lying two

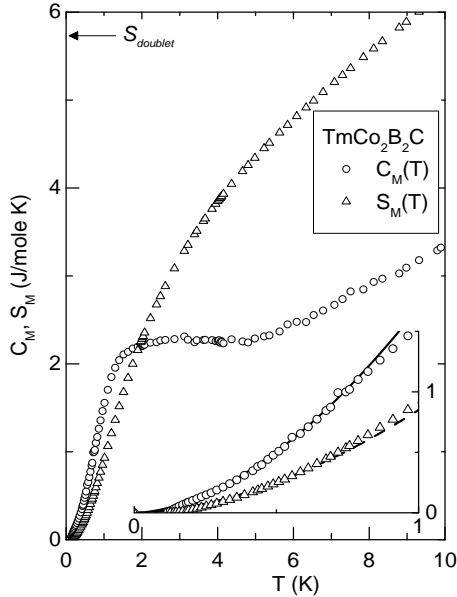


FIG. 8: The magnetic contribution to the specific heat (circles) and magnetic entropy (triangles) of $\text{TmCo}_2\text{B}_2\text{C}$. The expected entropy for a doublet is shown as a horizontal arrow. The inset shows, on an expanded scale, the experimental curves together with their low-temperature fits: $C_M(T)=1.7T^{7/4}$ J/moleK (solid line) and $S_M(T)=0.85T^{7/4}$ J/moleK (dashed line).

levels of Tm^{3+} are separated from the highest ones by an energy gap which must be much higher than 8 K: indeed inelastic neutron scattering on the isomorphous $\text{TmNi}_2\text{B}_2\text{C}$ showed that the doublet ground-state is separated from the first excited-state by 30 K.^{23,24,25,26} We have carried out preliminary inelastic neutron measurements on BT-7 to search for crystal field excitations in $\text{TmCo}_2\text{B}_2\text{C}$. We did not find any sharp excitations up to an energy transfer of 20 meV, but we did observe at 4.0 K a distribution of scattering (not shown) that appeared quasi-elastic, with the energy resolution of 1.0 meV employed. The wave vector and temperature dependence of this scattering indicated that it was magnetic in origin, and fitting with a Lorentzian distribution gave a half width $\Gamma=3.9(4)$ meV. Further studies are underway.

As seen in Fig. 2(b), the $C(T)$ curve of the rq $\text{TmNi}_2\text{B}_2\text{C}$ manifests the magnetic phase transition as a broadened and weak magnetic event. Along the same line of reasoning, the shoulder-like region in Figs. 7-8 is considered to be the region within which the magnetic phase transition of $\text{TmCo}_2\text{B}_2\text{C}$ sets-in (see the last comment in § II.B). Then the critical temperature is taken to be the point of the maximum slope which is found to be 0.8 K, in

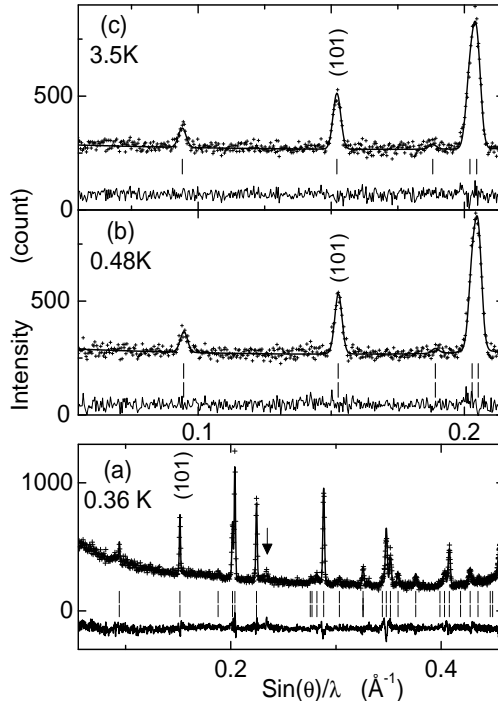


FIG. 9: Neutron-diffractograms of $\text{TmCo}_2\text{B}_2\text{C}$, measured at (a) NIST high resolution diffractometer, $\lambda=2.0787 \text{ \AA}$, and (b, c) NIST triple axis diffractometer $\lambda=2.359 \text{ \AA}$. The small vertical arrow indicates an impurity peak (see Figs. 1 and 3). A noticeable increase in the low angle intensities can be observed in lower panel but not in the upper panels: this suggests that this broadening is instrument-dependent and not due to a small angle scattering arising from magnetic or structural disorder induced by the rapid quench process.

excellent agreement with the considerations of Figs. 4-6.

D. Neutron diffraction

The high-resolution neutron diffractograms (Fig. 9) have been measured on BT-1 down to 0.36 K using a He3 cryostat and for as low angle as possible. Within the measured temperature range and experimental accuracy, no additional Bragg peaks that might be associated with magnetic order are observed. We therefore carried out diffraction measurements using the high-intensity/coarse resolution thermal triple axis instruments BT-9 and BT-7 to search for magnetic order. Within the angular range up to 65 degrees in scattering angle, the only significant change in intensity was observed for the (101) Bragg peak, as shown by the

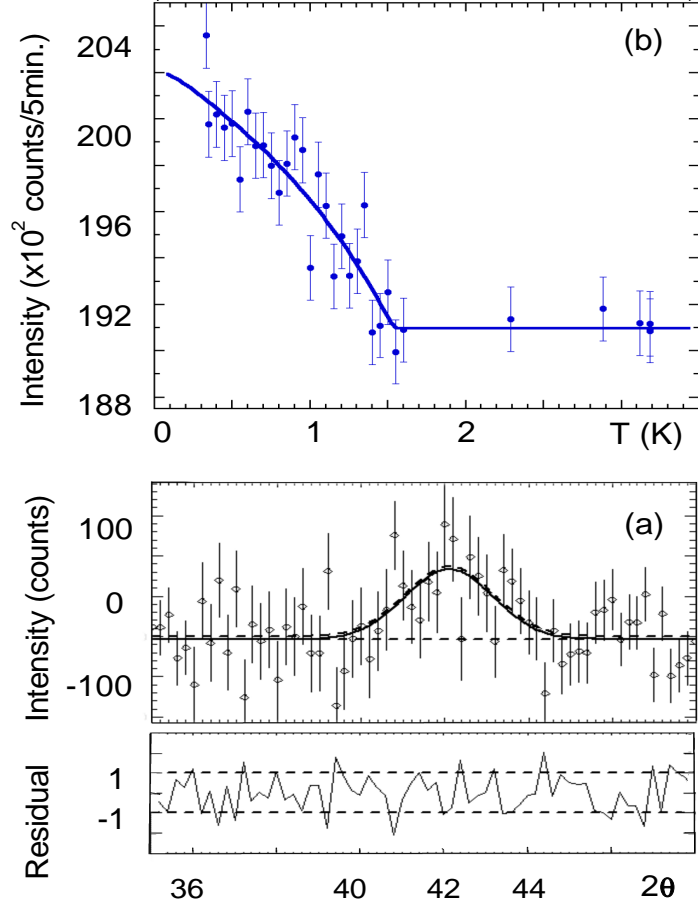


FIG. 10: (a) The difference pattern of the (101) peak obtained after subtracting the intensities measured at 4.0 K from those measured at 0.45 K. The line is a Gaussian fit to the experimental points (the residual graph represents the difference between the fit and the data). (b) Thermal evolution of the intensity of the (101) Bragg peak. Each point represents a measurement of the peak using a single setting of the Position Sensitive Detector on BT-7. The solid curve is a fit to mean field theory; this gives a critical temperature of 1.54(8) K. Error bars in this figure are statistical and represent one standard deviation.

difference plot in Fig. 10 (a). The temperature dependence of the intensity of this peak is shown in Fig. 10 (b), and the increase at lower temperatures indicates that magnetic order has developed. The solid curve is a fit of mean field theory to the data, which indicates that the magnetic ordering temperature is 1.54 K; this critical point (though determined from mean field analysis which is not well suited for such a determination) is nearly twice the value estimated from the susceptibility (Fig. 5) and the specific heat (Fig. 7). Considering

that the rq process is observed to induce a drastic broadening in the transition region (see Fig. 2), then it is most probable that the difference in the values of the transition point is due to the fact these techniques are differing in their frequency window.

The observation of a magnetic contribution at the (101) peak suggests that the magnetic wave vector is (000). It is emphasized that the weak impurities do not influence this analysis since we used the subtraction method (see Fig. 10). Below we argue that the only magnetic structure which is compatible with this (000) wave vector is the FM state. Such a conclusion is consistent with the above mentioned arguments about the forced magnetization (Fig. 6) and the magnon contribution of the specific heat (Fig. 7). As the crystal structure is body centered tetragonal (no orthorhombic distortion is expected since magnetostriction effects are weak) with only one Tm atom per primitive cell, then no order of the Tm sublattice can be antiferromagnetic. However, there are two Co atoms per primitive cell and as such an AFM order may develop but this should be discarded since there are no magnetic moments on the Co sublattice (see above). Thus it is concluded that this magnetic order must be due to the FM order of the Tm sublattice: it is recalled that both the saturated and effective moments are in excellent agreement with those found for $\text{TmNi}_2\text{B}_2\text{C}$. It is worth adding that our recent studies show that the manifestation of a FM state in $\text{TmCo}_2\text{B}_2\text{C}$ is not unusual: a FM state is common among the magnetic $R\text{Co}_2\text{B}_2\text{C}$ compounds ($R=\text{Dy, Ho, Er}$)²⁷ and $\text{TbCo}_2\text{B}_2\text{C}$.²⁸

On comparing the obtained results of $\text{TmCo}_2\text{B}_2\text{C}$ with those of $\text{TmNi}_2\text{B}_2\text{C}$, it is evident that their magnetic ground state are different: the former manifests a colinear FM state while the later orders into a modulated spin density wave. This difference is attributed to the difference in the indirect exchange couplings which in turn is due to the difference in the electronic structures. It is recalled that there is a clear difference between the electronic structure of $\text{LuNi}_2\text{B}_2\text{C}$ and $\text{LuCo}_2\text{B}_2\text{C}$.²⁹ On the other hand, the observation that their magnetic moments are similar is an indication that the CEF properties of the Tm^{3+} ions have not been greatly modified by the rq process or by the interchange of the $3d$ atoms.

$\text{TmCo}_2\text{B}_2\text{C}$ shows no trace of superconductivity in the ac -susceptibility (down to 20 mK), the specific-heat (down to 100 mK), or the preliminary resistivity curves measured down to 20 mK (not shown). It is recalled that none of the reported members of the $R\text{Co}_2\text{B}_2\text{C}$ series is a superconductor,⁹ not even $\text{YCo}_2\text{B}_2\text{C}$ in spite of having a Sommerfeld constant and Debye temperature that are almost equal to those of superconducting $\text{YNi}_2\text{B}_2\text{C}$; $\text{YCo}_2\text{B}_2\text{C}$

manifests spin fluctuation features,¹⁶ a property assumed to be unfavorable to the onset of the superconductivity. These spin fluctuation (associated with the Co sublattice) together with the presence of the FM state (associated with the Tm sublattice) are detrimental to the presence of the superconductivity in TmCo₂B₂C.

IV. CONCLUSION

A single-phase TmCo₂B₂C has been successfully stabilized via the rapid-quench process. Its crystal structure is isomorphous to that of the body-centered tetragonal TmNi₂B₂C. The paramagnetic properties are characterized by a modified CW behavior while the low-temperature features are dominated by an ordering of Tm³⁺ moments. Based on the character of the low-temperature magnon contribution to the specific heat, the characteristic feature of the low-temperature forced magnetization, and the analysis of the magnetic contribution to the neutron diffractograms, it is inferred that the magnetic order of the Tm sublattice is FM. At 0.65 K and under an applied magnetic field of 150 kOe, the Tm³⁺ moment is observed to reach $4.5 \pm 0.2 \mu_B$; though only 65% of the value expected for a free Tm³⁺ ion, this value is only 6% lower than the moment of TmNi₂B₂C: it is concluded then that the CEF effects in both isomorphs are similar. Finally, no superconductivity is observed in TmCo₂B₂C down to 20 mK: a feature attributed to the presence of the spin fluctuation in the Co subsystem and the FM ordering of the Tm sublattice..

Acknowledgments

We acknowledge the partial financial support from the Brazilian agencies CNPq (485058/2006-5) and Faperj (E-26/171.343/2005). Identification of commercial equipment in the text is not intended to imply recommendation or endorsement by National Institute of Standards and Technology. We would like to thank Jiying Li for his assistance with the data analysis using the position sensitive detector on BT-7.

¹ B. Coqblin, *The Electronic Structure of Rare-Earth Metals and Alloys: The Magnetic Heavy Rare-Earth* (Academic Press, New York, 1977).

- ² D. Bloch and R. Lemaire, Phys. Rev. B **2**, 2648 (1970).
- ³ D. Bloch, D. M. Edwards, M. Shimizu, and J. Voiron, J. Phys. F: Metal Phys. **5**, 1217 (1975).
- ⁴ M. Cyrot and M. Lavagna, J. Phys. (Paris) **40**, 763 (1979).
- ⁵ J. Inoue and M. Shimizu, J. Phys. F: Metal Phys. **18**, 2487 (1988).
- ⁶ H. Eisaki, H. Takagi, R. J. Cava, B. Batlogg, J. J. Krajewski, W. F. Peck, K. Mizuhashi, J. O. Lee, and S. Uchida, Phys. Rev. B **50**, R647 (1994).
- ⁷ B. K. Cho, P. C. Canfield, and D. C. Johnston, Phys. Rev. Lett. **77**, 163 (1996).
- ⁸ J. W. Lynn, S. Skanthakumar, Q. Huang, S. K. Sinha, Z. Hossain, L. C. Gupta, R. Nagarajan, and C. Godart, Phys. Rev. B **55**, 6584 (1997).
- ⁹ M. ElMassalami, M. S. DaCosta, R. E. Rapp, and F. A. B. Chaves, Phys. Rev. B **62**, 8942 (2000).
- ¹⁰ M. El Massalami, E. F. Chagas, and R. E. Rapp, J. Magn. Magn. Mater **226-230**, 1058 (2001).
- ¹¹ H. Takeya, K. Togano, Y. S. Sung, T. Mochiku, and K. Hirata, Physica C **408**, 144 (2004).
- ¹² T. Siegrist, H. W. Zandbergen, R. Cava, J. J. Krajewski, and W. F. Peck, Nature (London) **367**, 254 (1994).
- ¹³ T. Siegrist, R. Cava, J. J. Krajewski, and W. F. Peck, J. Alloys Compd. **216**, 135 (1994).
- ¹⁴ B. K. Cho, M. Xu, P. C. Canfield, L. L. Miller, and D. C. Johnston, Phys. Rev. B **52**, 3676 (1995).
- ¹⁵ R. Movshovich, M. F. Hundley, J. D. Thompson, P. C. Canfield, B. K. Cho, and A. V. Chubukov, Physica C **227**, 381 (1994).
- ¹⁶ M. El Massalami, H. A. Borges, H. Takeya, R. E. Rapp, and A. Chaves, J. Magn. Magn. Mater. **279**, 5 (2004).
- ¹⁷ L. J. Chang, C. V. Tomy, D. M. Paul, and C. Ritter, Phys. Rev. B **54**, 9031 (1996).
- ¹⁸ A. M. Mulders, P. C. M. Gubbens, and K. H. J. Buschow, Phys. Rev. B **54**, 14 963 (1996).
- ¹⁹ A. M. Mulders, P. C. M. Gubbens, U. Gasser, C. Baines, and K. H. J. Buschow, Phys. Rev. B **57**, 10 320 (1998).
- ²⁰ B. Holmstrom, A. C. Anderson, and M. Kruis, Phys. Rev. **188**, 888 (1969).
- ²¹ M. El Massalami, R. E. Rapp, F. A. B. Chaves, H. Takeya, and C. M. Chaves, Phys. Rev. B **67**, 224407 (2003).
- ²² M. El Massalami, R. E. Rapp, and H. Takeya, in *Studies in High Temperature Superconductors*, edited by A. Narlikar (Nova Science, New York, 2003), vol. 45.

- ²³ U. Gasser, P. Allenspach, J. Mesot, and A. Furrer, *Physica C* **282-287**, 1327 (1997).
- ²⁴ U. Gasser, P. Allenspach, F. Fauth, W. Henggeler, J. Mesot, A. Furrer, S. Rosenkranz, P. Vorderwisch, and M. Buchgeiste, *Z. Phys. B* **101**, 345 (1996).
- ²⁵ M. Rotter, C. Sierks, M. Loewenhaupt, J. Freudenberger, and H. Schober, in *Rare Earth Transition Metal Borocarbides (Nitrides): Superconducting, Magnetic and Normal State Properties*, edited by K. H. Müller and V. Narozhnyi, Nato Advanced Research Workshop (Kluwer Academic, 2001), pp. 137–153.
- ²⁶ U. Gasser, P. Allenspach, A. Furrer, and A. M. Mulders, *J. Alloys and Compd* **257-277**, 587 (1998).
- ²⁷ M. ElMassalami, R. Moreno, H. Takeya, B. Ouladdiaf, J. W. Lynn, and R. S. Freitas, *J. Phys: Condens Matter* (2008), submitted.
- ²⁸ M. ElMassalami, R. Moreno, R. M. Saeed, F. A. Chaves, H. Takeya, B. Ouladdiaf, and M. Amara, *J. Phys: Condens Matter* **21** (2008), (submitted).
- ²⁹ R. Coehoorn, *Physica C* **228**, 331 (1994).